

Modeling of C_2 addition route to cage closure and formation of C_{60}

Sabih D. Khan¹ and Shoaib Ahmad²

¹NILOP, PINSTECH, Islamabad, Pakistan.

E-mail: sabih@lahorebiz.com

²National Centre for Physics, QAU Campus, Shahdara Valley Road, Islamabad 44000, Pakistan

Email: sahmad.ncp@gmail.com

Abstract

To understand the phenomenon of fullerene growth during synthesis, an attempt is made to model a minimum energy growth mechanism using semi-empirical quantum mechanics code. C_2 addition by the close-caged and open-caged routes is modeled. The growth of C_{20} fullerene, graphene and corannulene is also modeled. C_{20} corannulene formation is identified as a major step in the growth process. Growth prior to this is followed by an open-caged route, while after C_{20} corannulene formation the growth is progressed by close-caged route. A predicted mechanism for transition from open-caged C_{24} to close-caged C_{24} is also modeled. However, this transition needs to be further investigated. C_{60} is the most stable fullerene for $n < 60$ and C_{20} fullerene is energetically less stable as compared to C_{20} corannulene. Other growth mechanisms could also occur in energetic environment commonly encountered in fullerene synthesis, but our purpose was to identify a minimal energy route, that is the most probable route.

Keywords: Buckyball growth, buckyball fragmentation, fullerene synthesis, semi-empirical quantum mechanics, MNDO.

PACS: 31.15.Ct, 81.05.Tp, 82.20.Wt

1. Introduction

Nanotechnology could be classified as design efforts to model and simulate various nano-sized machines and as implementation efforts to realize that these design as final fabricated devices and components. Molecular modeling is a tool which is required in both of the efforts; at the design stage it has the role of the paint brush and canvas, while in implementation effort it would allow nanotechnologists to simulate and model the sequence of atomic manufacturing by adding atoms or molecules one by one. This communication could be considered a part of the effort to re-evaluate methods of quantum physics and apply them to molecules.

2. Molecular Modeling Methods

In efforts to apply quantum physics to nano-scale objects a large number of techniques have been explored so far, which could be classified as static and dynamic molecular modeling. Static modelings involve attempts to solve time-independent Schrödinger wave equation, while dynamic modeling necessitates solving the time-dependent Schrödinger wave equation. Ab initio methods involve solutions with minimum approximations, while semi-empirical solutions use approximate parameterized values of several integrals, the parameterization is mostly obtained from experimental results or ab initio solutions. Quantum Monte Carlo (QMC) is yet another method which attempts to solve molecular systems stochastically, but whose results are so accurate that they are usually considered exact. When it comes to modeling even the simplest and smallest nano-clusters both ab initio and QMC requires extremely fast processing and very large storage systems, hence super computers are required. Semi-empirical methods on the contrary require less computational effort but provide results within certain tolerance. Semi-empirical modeling at the starting stages and ab initio or QMC at the final stages of nano-machine designing provides an optimum route. Drexler has proposed yet another route [1] that is to initially model molecules using molecular mechanics (a highly simplified molecular modeling method) at the initial stage while advanced techniques at the final stage. The dynamic methods on the other hand are much more computationally expensive and usually require tools like molecular dynamics (MD) [2], first principle molecular dynamics (FPMD) [3], etc. Dynamic methods take into account the molecular vibrations, rotations, etc. in addition to molecular instabilities due to electronic interactions. We have selected semi-empirical methods for our computational nanotechnology research based on its efficiency to model nano-clusters in less time and with considerable accuracy.

3. Parameterization based Semi-empirical Methods (MNDO, AM1, PM3)

The three most commonly used semi-empirical methods are MNDO [4], AM1 [5] and PM3 [6], which have certain common features. They are all self-consistent field (SCF) methods, they take into account electrostatic repulsion and exchange stabilization, and, in them, all calculated integrals are evaluated by approximate means. Further, they all use a restricted basis set of one *s* orbital and three *p* orbitals (*p_x*, *p_y*, and *p_z*) per atom and ignore overlap integrals in the secular equation. Thus, instead of solving $|H - ES| = 0$ the expression $|H - E| = 0$ is solved, in which *H* is the secular determinant, *S* is the overlap matrix, and *E* is the set of eigenvalues. These approximations considerably simplify quantum mechanical calculations on systems of chemical interest. As a result, larger systems can be studied [7].

All these semi-empirical methods contain sets of parameters. MNDO, AM1 and PM3 use single-atom parameters. Not all parameters are optimized for all methods; for example, in MNDO and AM1 the two electron one center integrals are normally taken from atomic spectra. In the list given in Table 1 [8], parameters are either optimized for a given method or the value of the parameter was obtained from experiment. Where neither information is given, the associated parameter is not used in that method. The three semi-empirical methods also use two experimentally determined constants per atom: the atomic mass of the most abundant isotope and the heat of atomization. MNDO, AM1 and PM3 belong to the family of NDDO (Neglect of Diatomic Differential Overlap) methods. In these methods all terms arising from the overlap of two atomic orbitals which are on different centers or atoms are set to zero [7].

4. Benchmarking for Fullerenes

Fullerene electronic structures differ from conventional carbon structure in hydrocarbons, on which most of the parameterization methods are based on; in the former case the carbon-carbon network forms a curved structure. The parameterization methods may not be entirely accurate for fullerenes. We have employed a brute force approach and compared the results of geometry optimization with those of the experimentally reported results. Table 2 presents the output of geometry optimization calculations carried out by the three parameterization methods i.e. MNDO, AM1 and PM3, and this when compared with the experimental results [9] indicates that the MNDO method is more accurate at least for this case of fullerene modeling, i.e. it has the lowest norm of 1.055545. Additionally, MNDO have been a favorite method for fullerene modeling by various researchers [10-12].

5. Justification for C₂ Insertion based Growth

C₆₀ growth can be modeled using C₁, C₂, C₃ or larger carbon molecules additions, but experimental observations from emission spectra of regenerative sooting discharge indicate C₂ to be an important constituent of carbonaceous plasma which lead to the formation of fullerenes [13]. Additionally Scheier et al. [14] also provides experimental evidence for the critical role of C₂ in fullerene fragmentation. We attempted to isolate the role of C₂ by modeling a hypothetical plasma with C₂ as the predominant species. A hypothetical model for the ingestion of two carbon atoms in a fullerene to fullerene conversion was first described by Endo and Kroto [15]. The parent fullerene C_n should have somewhere on its surface a patch consisting of two pentagons linked to opposite edges of a central hexagon, the ingestion process is illustrated in figure 1(a) and figure 1(b). If the appropriate set of three rings is present, an isolated-pentagon isomer of C_n can gain two atoms in this way, but the process yields what is presumably a high-energy form of C_{n+2} with fused pentagons. A further rearrangement is needed to give a final product that has isolated pentagons, Stone-Wales transformation is one such mechanism [10, 16], as illustrated in figure 1(c) and figure 1(d).

6. Criteria for Stability

The SCF calculation gives density matrix (P) and Fock matrix (F) as the result. The total electronic energy E_{elec} and core-core repulsion energy E_{nuc} can be calculated as follows [7]:

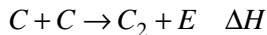
$$E_{elec} = \frac{1}{2} \sum_{\mu} \sum_{\nu} P_{\mu\nu} (H_{\mu\nu} + F_{\mu\nu})$$

$$E_{nuc} = \sum_A \sum_{B < A} E_N(A, B)$$

Where H is one-electron matrix, P is density matrix, F is Fock matrix and E_{nuc} is core-core repulsion integral. The sum of these two energies gives the energy released when the ionized atoms and valence electrons combine to form a molecule. If we also add energy required to ionize atoms and valence electrons E_{isol} and heat of atomization E_{atom} then the total sum would be heat of formation at room temperature:

$$\Delta H_f^{298} = E_{elec} + E_{nuc} + \sum_A E_{isol}(A) + \sum_A E_{atom}(A)$$

Heat of formation is the energy released when isolated atoms combine to form a stable molecule. From thermodynamic argument it could be proved that this excess energy released is actually the binding energy of the molecule. So for case of C₂ molecule formation:



$$\Delta H = -E$$

E = Energy Released During Formation = Binding Energy = -HoF

$$-\frac{\Delta H}{n} = \text{Binding Energy per Atom}$$

For fullerenes in which all atoms are similar HoF per carbon atom is approximately equal to the negative of binding energy per atom. Binding energy per atom is the energy required to remove a single atom from the molecule. The more tightly an atom is bound in a molecule, the more stable a molecule is, so on the basis of this argument, one can treat HoF per atom as a criteria for judging the molecular stability. The lower the value of HoF per atom, the more stable the molecule.

7. Results of Molecular Modeling

C₂ addition route for open-caged fragments and close-caged fragments were modeled using Semi-empirical Quantum Mechanical method (MNDO) and the heat of formation per carbon atom is presented in figure 2, where open-caged and close-caged routes are plotted by filled circles and filled squares respectively. 3D rotateable images are also available in MDL MOL file format as multimedia 1 and multimedia 2, respectively. Heat of formation per carbon atom for the most stable fullerene isomers as given by the Atlas of Fullerenes are also presented in figure 2 and are plotted by unfilled squares. The corresponding 3D rotateable images are available in MDL MOL file format as multimedia 3. The growth route of C₂₀ fullerene and C₂₀ graphene by C₂ additions is plotted in figure 2 by filled diamonds and unfilled diamonds respectively and their 3D rotateable images are also available in MDL MOL file format as multimedia 4 and multimedia 5 respectively. For detailed analysis the growth of C₂₀ as a Corannulene, Fullerene or Graphene sheet are presented in more detail in figure 3, from n = 4 to n = 20. The geometry optimized structures by MNDO method for each cluster are illustrated next to each data point. To elaborate

and clearly present results from study, the $n = 20$ up to $n = 60$ results are shown in figure 4. The geometry optimized structures again are plotted next to each data point. The predicted transformation route for C_{24} fragment in C_{24} fullerene is illustrated in figure 5. The geometry optimized structures are illustrated next to each data point and type of transformation is also indicated between each two consecutive data points. 3D rotateable images of this transformation are provided in MDL MOL file format as multimedia 6.

8. Growth of C_{60} by Open Caged Fragments

The C_{60} can grow either from C_2 by an open caged route or close caged route. The complete growth sequence is presented in figure 2 by filled circles, all energies are calculated by MNDO method as implemented by ArgusLab 1.3 [17]. The sequence can be divided into three distinct regions, i.e. from C_2 to C_{20} , from C_{20} to C_{24} and C_{24} to C_{60} . Up to $n = 18$ the structure is two dimensional and all atoms are sp^2 hybridized. The transition from sp^2 to sp^x takes place during C_{18} to C_{20} growth. The 1st sequence is illustrated in more detail in figure 3. It could be seen that as growth occurs from C_2 to larger molecules the Heat of Formation (HoF) per atom is decreased. A decrease in HoF indicates higher stability of the molecules, hence thermodynamics dictates the formation of larger carbon clusters from C_2 molecules. In the second region, i.e. C_{20} to C_{24} growth, HoF per atom increases during C_{22} and C_{24} formation. The thermodynamics tells that for growth to progress through this region some amount of energy is required. During fullerene synthesis in arc discharge [18], laser ablation [19], CVD [20] and even regenerative sooting discharge [21] a large distribution of energy exists and it could be possible that this excess energy required is obtained from the plasma. During the 3rd region the growth progresses similar to region 1, i.e. HoF per atom decreases with increasing size of cluster. As indicated in figure 4 and in the respective 3D rotateable images, at this stage open caged fragments grow with the addition of C_2 at the edges of the fragments, with C_2 axis in parallel to the tangential direction of the outer edge, until C_{50} open-caged fragment is reached. From C_{52} to C_{60} the C_2 's are added with C_2 axis perpendicular to the tangential direction of the outer edge. It appears that C_{20} to C_{24} transition is a crucial sequence of growth, which if overcome leads to C_{60} growth otherwise the growth may stop at corannulene. As evident from the HoF per atom of the molecular sequence, the HoF per atom decreases as number of carbon atoms is increased and C_{60} is the one with lowest HoF per atom, which is in line with experimental observations that C_{60} is the most abundant [22]. The growth of C_{60} is carried from C_2 additions by lower energy path, i.e. at each subsequent stage the molecule becomes more stable as it grows until C_{60} .

9. Growth of C₆₀ by Close Caged Fullerene

For the sake of comparison, the HoF calculated for open-caged fragments is compared with that of close-caged fullerenes. Since a closed cage structure does not exist with 1 hexagon and 12 pentagons ($h = n/2 - 10$ Goldberg Polyhedra) [10], therefore C₂₂ does not exist, thus with C₂ addition we started from C₂₄ and went up to C₆₀. The only restrictions in the first case in modeling were that the structure should be close-caged and only hexagons and pentagons allowed. At this comparative stage not all structures were the most symmetric isomers, however, maximum attempts were carried out to make C₂ insertions in such a way as to yield more symmetric isomers. For the sake of a more thorough comparison, HoF of the most stable isomers as identified by Fowler [10] were also calculated. Geometry optimized structures of these close-caged systems are illustrated in figure 4, the corresponding HoF per atom are plotted against the open-caged fragments route. The growth sequence by this route needs to be further investigated in future with the transformation of less symmetric and less energetically favored isomers into more energetically favored isomers possibly by SW transformation. It could be observed quite clearly that HoF per atom of close-caged route above C₂₄ up to C₆₀ is lower than open-caged route. Thus above C₂₄ close-caged growth is more energetically favored than their corresponding open-caged fragments. But since in discharges there is a wide variation in plasma temperature and other experimental conditions, the slightly higher energy route i.e. open-caged fragments route might also occur but as soon as the fragments are extracted from the plasma and enter a low temperature region they might tend to convert into stable close-caged fullerenes by atomic rearrangement, hence only close-caged fullerenes are detected experimentally.

10. C₂₀ Growth

From the analysis so far it appears that the growth of C₆₀ below C₂₄ also needs to be explored further. So for comparison of C₂₀ corannulene growth sequence with other routes, an attempt was made to model the growth of two other rival C₂₀ molecules i.e. C₂₀ fullerene and C₂₀ graphene sheet. C₂₀ corannulene growth for $n = 4$ to $n = 20$ is given by molecules E2 till E10 in figure 3. In case of C₂₀ fullerene, since C₂₀ is the smallest known close-caged fullerene so only possible route that came immediately to mind was by open-caged route. Up to C₁₀ the growth sequence is similar to C₂₀ corannulene and is illustrated in figure 3, afterward the new C₂ molecules were inserted with C₂ axis perpendicular to the tangential axis of the outer most ring, this keeps on until the cage is closed. The sequence from C₁₂ to C₂₀ is illustrated in figure 3 by molecules F6, F7, F8, F9 and F10. The HoF per atom of the sequence is also presented in figure 3 by the data points with filled squares. C₂₀ graphene growth is illustrated in figure 3 and HoF per atom is

given by data points with unfilled squares. The growth sequence is similar to C_{20} corannulene and fullerene up to C_8 , afterward the growth continues by a slightly different isomer represented by G5 and grows into G10 – the C_{20} graphene.

A close analysis of C_{20} growth in the figure 3 indicates that C_{20} corannulene growth sequence appears to be the most stable growth sequence as it has the lowest HoF per atom. This is in line with other researchers work, i.e. detailed theoretical studies on C_{20} fullerene using Quantum Monte Carlo have indicated that C_{20} is at the cross-over of stability [23].

11. Final Picture

It appears that initially, based on our calculated values of HoF per atom and the thermodynamic considerations, growth is progressed by the open-caged fragments route up to C_{20} , and after C_{24} , the growth appears to be more favored by close caged fullerene route. During C_{20} to C_{24} a transition from open caged fragments to close caged fullerenes occur which further needs to be investigated. As a test case we have worked out on possible sequence for this transition and is illustrated in figure 5. It appears that for a C_{20} corannulene to C_{24} fullerene conversion the path of lower HoF per atom with increasing number of carbon atoms appears to be violated. While room is still open for working out the most energetically favored conversion route, but in a crude analysis it appears that a finite amount of energy has to be available in the environment for the jump from the curved C_{20} to the close caged C_{24} . If however such energy is not available then C_{20} corannulene might grow into some other structure like nanotubes or its growth may stop. Recently, one of us has presented growth selection criteria between fullerenes and nanotubes by continuum elasticity model and rotations of growing molecules [24]. Our current work hypothesizes yet another selection criterion between fullerenes and nanotubes, i.e. if sufficient environment is available for the transformation of C_{20} into C_{24} fullerene then C_{60} growth will be more probabilistic.

12. Conclusion

Based on HoF per atom calculated computationally using MNDO method it appears to be that initially C_{60} grow from C_2 by C_2 addition sequence up to C_{20} by open caged fragments, a transition occurs from open caged fragments into close caged fullerenes during C_{20} and C_{24} , after C_{24} the growth progresses up to C_{60} by close caged fullerenes with C_2 insertion mechanism. Other rival but energetically less favored growth routes do exist and could also be taking place, but experimental studies appears to be in favor of C_{60} growth by close caged fullerenes. The

transition between C_{20} and C_{24} needs to be further investigated, to identify the most energetically favored transition mechanism. C_{60} is the most stable amongst all fullerenes and clusters as it has the lowest HoF per atom. C_{20} fullerene is an unstable molecule as compared to C_{20} corannulene.

Acknowledgments

The authors would like to thank Ministry of Science and Technology, Pakistan for their funding in our project Carbon based Nanotechnology. We would also like to thank our team members Sohail Ahmad Janjua, Shahid Nawaz, Mashkoor Ahmad, Rahila Khalid, Abid Aleem and Bashir Ahmad for their continual support in our theoretical work. We would especially like to thank Dr. Talat S. Rahman (KSU, USA), Dr. Sikander M. Mirza (PIEAS, Pakistan), Dr. Muhammad Mansha (PIEAS, Pakistan), Dr. Rashid Ahmad (PINSTECH, Pakistan), Ms. Tania Jabar (PINSTECH, Pakistan) and Dr. Mazhar Mehmood (PIEAS, Pakistan) for their helpful discussions related with molecular modeling, theoretical chemistry and thermodynamics. The appreciation and encouragement from Dr. Ghulam Murtaza, Dr. Kamal uddin and their colleagues at Pakistan Physical Society could also not be forgotten.

References

- [1] Drexler K. E. 1992 *Nanosystems; Molecular machinery, manufacturing and computation* (Wiley Interscience) chapter 3
- [2] Hinchliffe A. 1999 *Chemical Modeling; From Atoms to Liquids* (West Sussex: John Wiley & Sons Ltd.) 183-190
- [3] Car R. & Parrinello M. 1985 *Physical Review Letters* **55** 2471
- [4] Dewar M. J. S. & Thiel W. 1977 *JACS* **99** 4899-4907
- [5] Dewar M. J. S., Zebisch E. G., Healy E. F. & Stewart J. J. P. 1985 *JACS* **107** 3902-3909
- [6] Stewart J. J. P. 1989 *J. Comp. Chem.* **10** 209-220
Stewart J. J. P. 1989 *J. Comp. Chem.* **10** 221-264
- [7] Drakos N., Hennecke M., Moore R., Swan H., Lippmann J., Rouchal M. and Wilck M. 1998 MOPAC Manual (<http://home.att.net/~mopacmanual/node7.html>).
- [8] Drakos N., Hennecke M., Moore R., Swan H., Lippmann J., Rouchal M. and Wilck M. 1998 MOPAC Manual (<http://home.att.net/~mopacmanual/node441.html>).
- [9] Haddon R. C. 1993 *Science* **261** 1545-1550
- [10] Fowler P. W. & Manolopoulos D. E. 1995 *An Atlas of Fullerenes* (New York: Oxford University Press Inc.) pages 73 120-125 15-17 76-77

- [11] Weltner Jr. W. & Zee R. J. V. 1989 *Chem. Rev.* **89** 1713-1747
- [12] Plater J., Rzepa H. S., Stoppa F. and Stossel S. 1994 *J. Chem. Soc. Perkin Trans* **2** 399
- [13] Ahmad S., Qayyum A., Akhtar M. N. & Riffat T. 2000 *Nuclear Instruments & Methods in Physics Research B* **1-7**
- [14] Scheier P., Dunser B., Worgotter R., Muigg D., Matt S., Echt O., Foltin M., Mark T. D. 1996 *Physical Review Letters* **77** 2654-2657
- [15] O'Brian S. C., Heath J. R., Curl R. F. & Smalley R. E. 1988 *J. Chem. Phys.* **88** 220
- [16] Stone A. J. & Wales D. J. 1986 *Chem. Phys. Lett.* **128** 501
- [17] Thompson M. A., Zerner M. C. 1991 *J. Am. Chem. Soc.* **113** 8210
 Thompson M. A., Glendening E. D. & Feller D. 1994 *J. Phys. Chem.* **98** 10465-10476
 Thompson M. A. & Schenter G. K. 1995 *J. Phys. Chem.* **99** 6374-6386
 Thompson M. A. 1996 *J. Phys. Chem.* **100** 14492-14507
- [18] Kratschmer W., Lamb L. D., Fostiropoulos K. & Huffman D. R. 1990 *Nature* **347** 354
- [19] Ying Z. C., Hettich R. L., Compton R. N. and Haufler R. E. 1996 *J. Phys. B: At. Mol. Opt. Phys* **29** 4935-4942
- [20] Dresselhaus M. S., Dresselhaus G., Avouris P. (Eds.) 2001 *Topics Appl. Phys.* **80** 32-44
- [21] Ahmad S. 2001 *Eur. Phys. J. D* **15** 349-354
- [22] Kroto H. W., Heath J. R., O'Brien S. C., Curl R. F. & Smalley R. E. 1985 *Nature* **318** 162
- [23] Kent P. R. C., Towler M. D., Needs R. J. and Rajagopal G. 2000 *Physical Review B* **62** 15394
- [24] Ahmad S. 2005 *Nanotechnology* **16** 1739

Figure Captions

Figure 1. Fullerenes may grow by C_2 insertion which introduces a hexagon with every insertion, the unstable isomers may then be converted into stable ones by transformations like Stone-Wales transformation. (a) Two pentagons and central hexagon before C_2 insertion, (b) C_2 insertion leading to addition of new hexagon, (c) Pyracylene / Pyracene patch which can undergo SW transformation, (d) Pyracylene / Pyracene patch after SW transformation.

Figure 2. Growth of C_2 into C_{60} by C_2 insertion, for $n=2$ to 20 energies of C_{20} fullerene, graphene and corannulene growth is presented and for $n > 20$ C_{60} energies of growth by open-caged fragments and close-caged fullerenes route is presented. All energies are calculated using MNDO method.

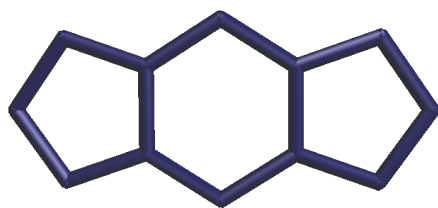
Figure 3. Growth of C_{20} Corannulene, Fullerene and Graphene is modeled from C_4 up to C_{20} . HoF per carbon atom as a function of number of carbon atoms is also presented.

Figure 4. Growth of C_{60} from C_{24} is modeled by both open-caged fragments and close-caged fullerene routes. HoF per carbon atom as a function of number of carbon atoms is also presented.

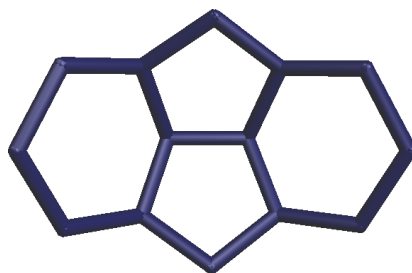
Figure 5. Predicted growth path of C_{24} fragment to C_{24} Fullerene Transformation. HoF per carbon atom is presented for all 13 molecules. Transformation type during each molecular transformation is also presented.

Table 1. Parameters used in Semi-empirical Methods.

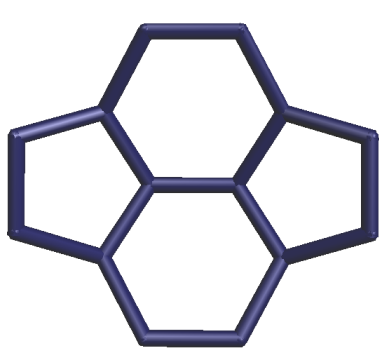
Table 2. Benchmarking of MNDO, AM1 and PM3 for C_{60} Fullerene.



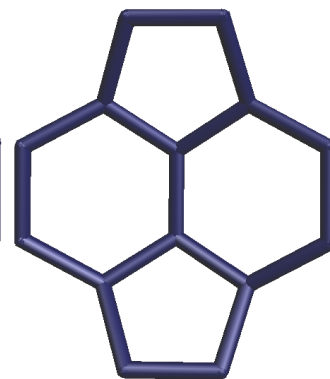
(a)



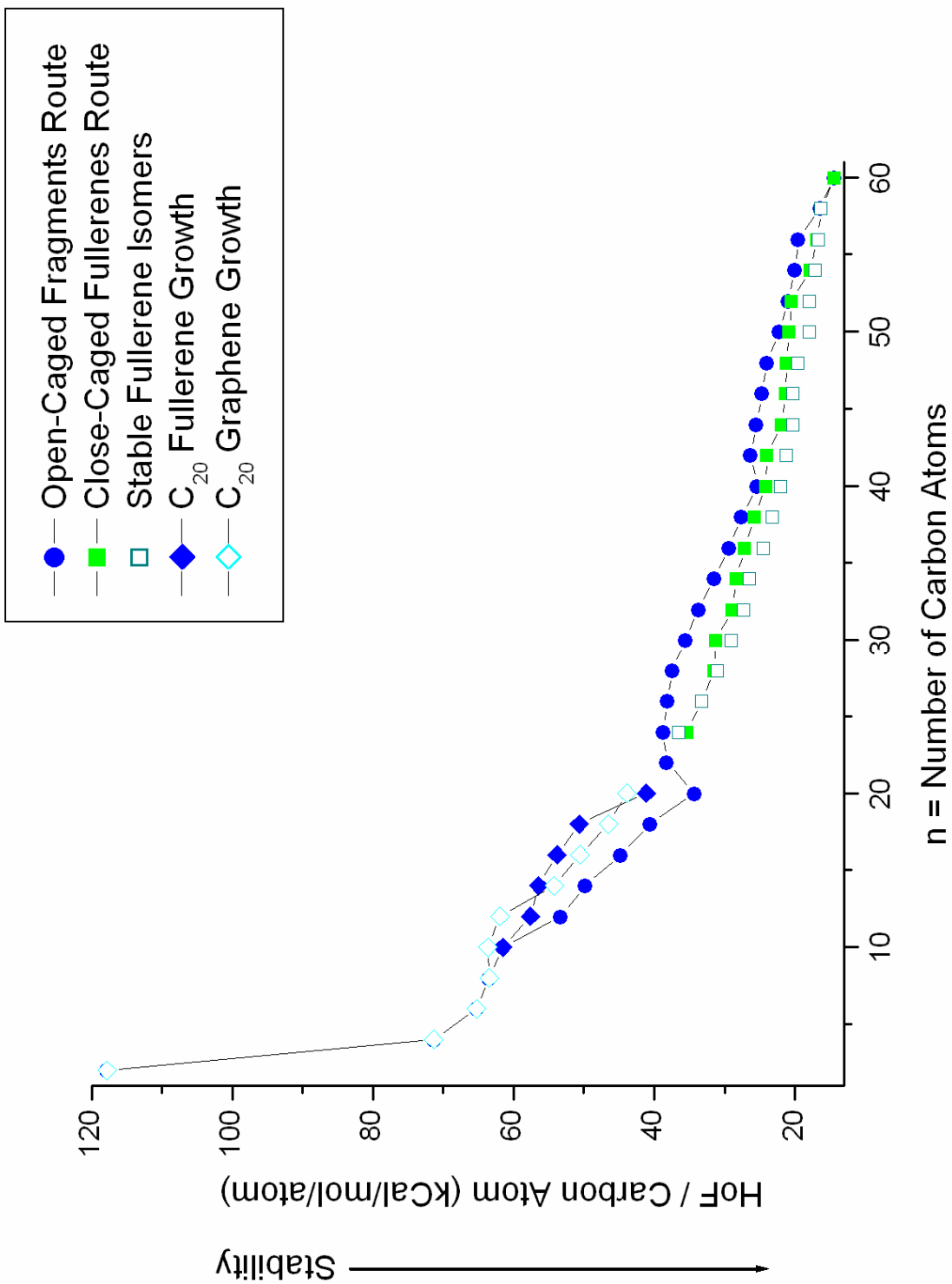
(b)

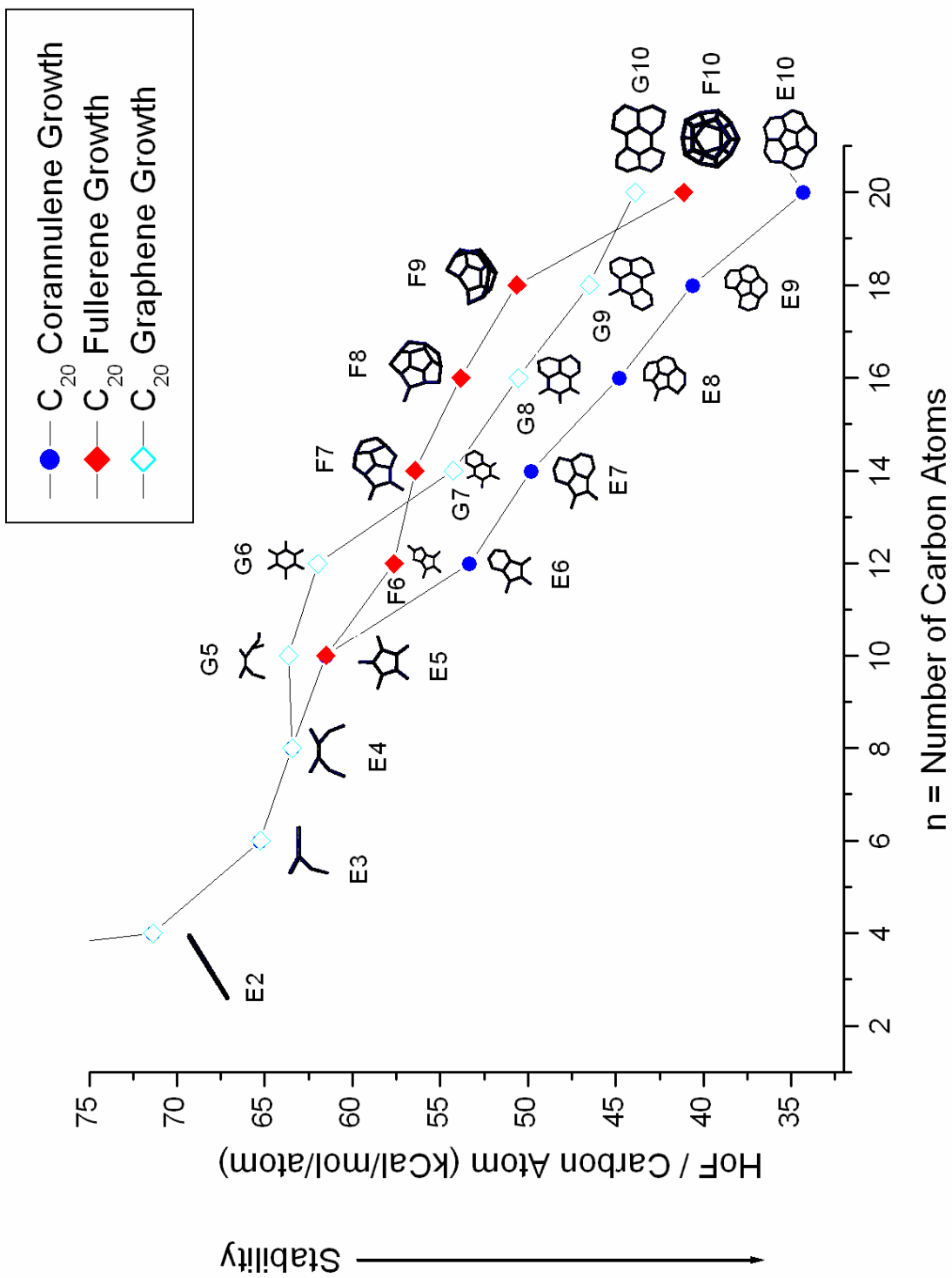


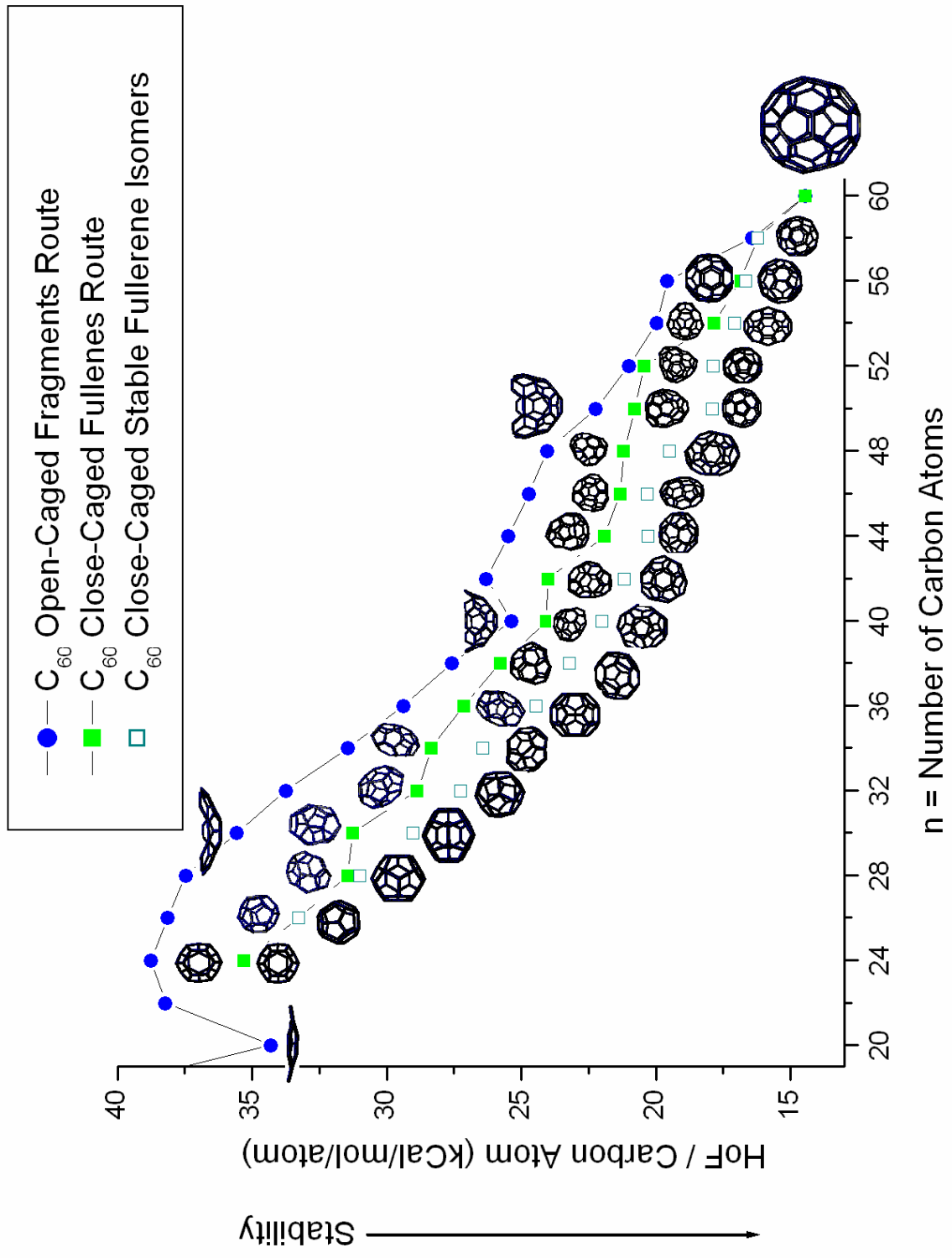
(c)



(d)







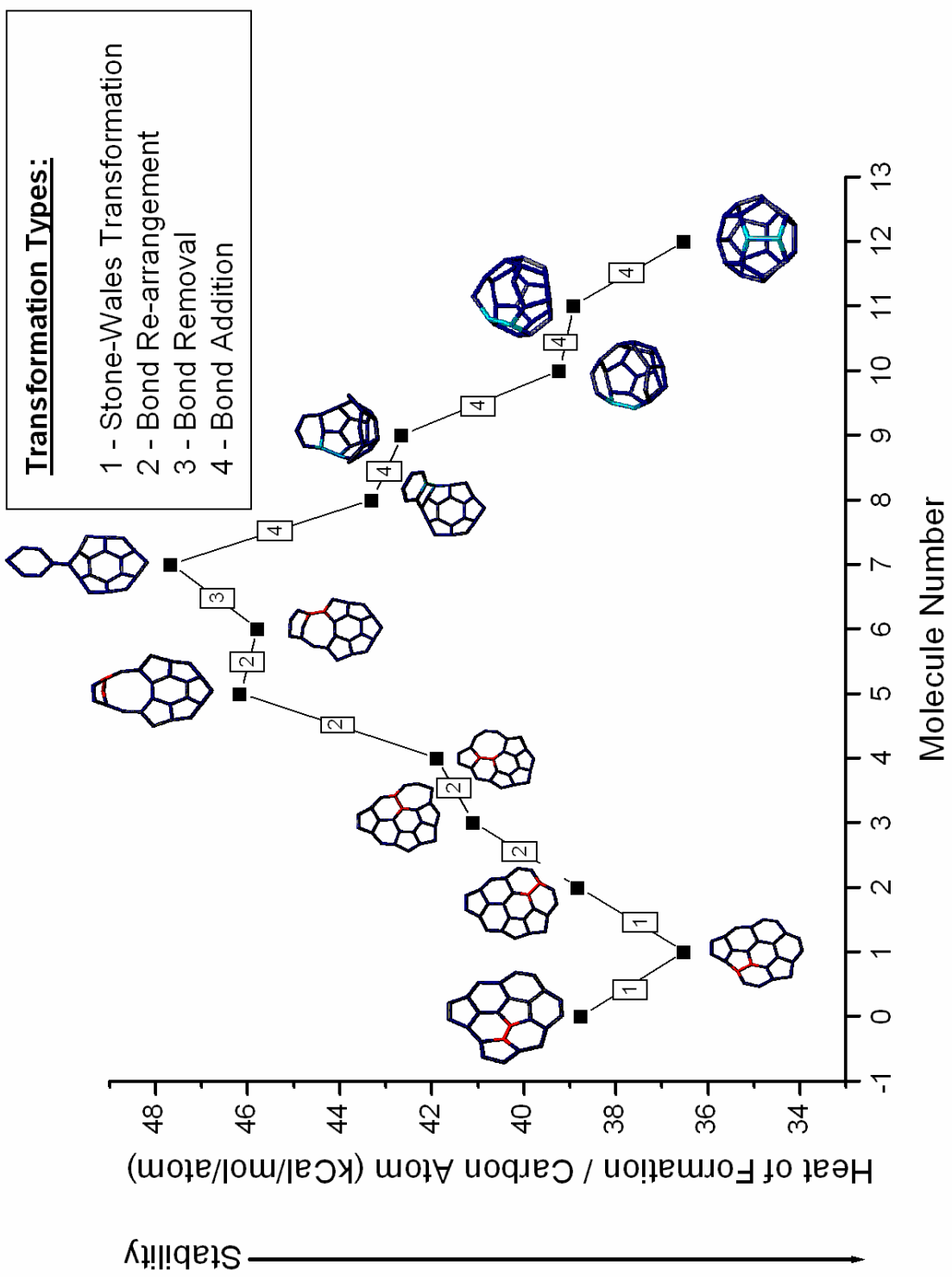


Table 1

Parameter	Description	MNDO	AM1	PM3
U_{ss} and U_{pp}	S and p atomic orbitals; one-electron one-center integral	Optimized	Optimized	Optimized
β_s and β_p	s and p atomic orbital one-electron two-center resonance integral terms	Optimized	Optimized	Optimized
ξ_s and ξ_p	s and p-type Slater atomic orbital exponent	Optimized	Optimized	Optimized
α_A	Atom A core-core repulsion term	Optimized	Optimized	Optimized
G_{ss}	s-s atomic orbital one center two electron repulsion integral	Experimental	Experimental	Optimized
G_{sp}	s-p atomic orbital one center two electron repulsion integral	Experimental	Experimental	Optimized
G_{pp}	p-p atomic orbital one center two electron repulsion integral	Experimental	Experimental	Optimized
$G_{pp'}$	p-p' atomic orbital one center two electron repulsion integral	Experimental	Experimental	Optimized
H_{sp}	s-p atomic orbital one center two electron exchange integral	Experimental	Experimental	Optimized
K_{nA} or a_{nA}	A Gaussian multiplier for n th Gaussian of atom A	-	Optimized	Optimized
L_{nA} or b_{nA}	A Gaussian exponent multiplier for n th Gaussian of atom A	-	Optimized	Optimized
M_{nA} or c_{nA}	A radius of center of n th Gaussian of atom A	-	Optimized	Optimized

Table 2

Method	Single Bond o (Å)	Error (%)	Double Bond o (Å)	Error (%)	Norm
Experimental	1.46		1.4		
[9]					
MNDO	1.475	1.027397	1.4	0	1.055545
AM1	1.465	0.342466	1.385	-1.07143	1.265242
PM3	1.459	-0.06849	1.384	-1.14286	1.310814